Submitted: November 20, 2024 **Revised: February 4, 2025** **Accepted: February 12, 2025**

Effect of high pressure torsion and annealing on the microstructure and microhardness of Inconel 718 produced by selective laser melting

K.S. Mukhtarova [1], **R.V. Shakhov** [2], **Sh.Kh. Mukhtarov** [2] ✉

[1] Eötvös Loránd University, Budapest, Hungary

[2] Institute for Metals Superplasticity Problems of RAS, Ufa, Russia

✉ shamilm@imsp.ru

ABSTRACT

Comparative study of Inconel 718 nickel-base superalloy produced by selective laser melting (SLM) and conventional technology was carried out. The SLM Inconel 718 microstructure consists of γ grains, surrounded by δ phase plates and small carbides. γ'' and γ' precipitates were present within the γ subgrains. The δ phase plates are mainly located along grain boundaries like in conventional Inconel 718. The γ grains consist of columnar and equiaxed subgrains. Study of microstructure showed that the columnar subgrains in their turn consisted of equiaxed subgrains. The SLM material features a developed substructure in γ grains, and dispersed precipitates, oxides along subgrain boundaries. SLM Inconel 718 and conventional Inconel 718 were subjected to high pressure torsion (HPT), which resulted in microstructure refining down to nanocrystalline size and partial dissolution of Nb containing γ'' and δ phases. δ phase particles were revealed more clearly after subsequent annealing at the temperature close to aging temperature like in conventional superalloy. Nanostructure of SLM Inconel 718 formed by HPT had duplex ($\gamma+\delta$) structure and was found to be thermally stable at 600 °C during 2 h. Annealing of the SLM Inconel 718 led to superior microhardness (956.46 HV), which was slightly higher than that of the conventional superalloy.

KEYWORDS

nickel-based superalloy • microstructure • grain • boundary • selective laser melting • severe plastic deformation high pressure torsion • nanostructure • annealing • microhardness

Funding. *The reported study was accomplished according to the state assignment of IMSP RAS (No. 124022900106-9).*

Acknowledgements. *The research was carried out using the equipment of the shared services center of the Institute for Metals Superplasticity Problems of Russian Academy of Sciences "Structural and Physical-Mechanical Studies of Materials".*

Citation: Mukhtarova KS, Shakhov RV, Mukhtarov ShKh. Effect of high pressure torsion and annealing on the microstructure and microhardness of Inconel 718 produced by selective laser melting. *Materials Physics and Mechanics*. 2025;53(1): 109–116.
http://dx.doi.org/10.18149/MPM.5312025_9

Introduction

The nickel-base superalloy Inconel 718, which can be exposed to high mechanical and thermal stresses, is commonly used in rocket and aircraft engines [1–3]. The phase composition, heat treatment and production technique determine its performance characteristics. For instance, selective laser melting (SLM) is a particular technique of rapid prototyping, 3D printing, or Additive Manufacturing (AM) designed to melt and fuse metallic powders with a high power-density laser [4–11]. SLM produces solid, simple or geometrically complex objects having a number of layers [4–7,11–13]. The AM process results in the formation of a complex heterogeneous microstructure, characterised by the precipitation of dispersed strengthening phases and oxides. This is due to the combination of multiple heating and rapid cooling during the manufacturing process [4,8,10,14–18]. Consequently, the microstructure of the SLM material differs from that of materials produced by conventional methods. The microstructure is comprised of contained columnar and cellular grains, as observed in previous studies [19–21]. The microstructure of conventional superalloy subjected to severe plastic deformation by high pressure torsion (HPT) has been refined to nanoscale [22,23]. HPT can enhance the diffusion and dissolution of precipitates [23]. The microstructure and microhardness of SLM Inconel 718 and the conventional alloy subjected to HPT and annealing were compared in this paper.

Materials and Methods

Inconel 718 Ni-based superalloy, produced by SLM, was received in the form of a bar with a square cross-section measuring 11 × 11 × 73 mm^3, which was built vertically. The SLM scanning parameters, including laser power, scanning speed, layer thickness, and the distance between the scanning tracks of the laser beam, were selected to minimize porosity in the produced material. Table 1 shows the chemical composition of Inconel 718 Ni-based superalloy produced by SLM. The chemical composition of the superalloy was specified in the material's technical specifications, and its major elemental concentrations were confirmed using an energy-dispersive X-ray spectroscopic analysis (EDS, Aztec, Oxford Instruments). The samples 8 mm in diameter and 0.7 mm in thickness were cut from the SLM alloy. These small discs were processed by HPT on 5 revolutions at room temperature [24] and subsequently annealed at 600 °C for 2 h.

Table 1. The chemical composition of the SLM Inconel 718 alloy (wt. %)

Cr	Fe	Mo	Co	Al	Ti	Nb	C	B	Ni
19.8	18.4	3.4	0.1	0.6	1.0	5.9	0.04	0.03	base

The microstructure investigation was carried out with the use of scanning electron microscopy (SEM) in backscattering electron (BSE) mode. The electron backscattered diffraction (EBSD) analysis performed with a scan-step of 1 μm was carried out by Tescan Mira-3. Channel 5 processing software was applied for EBSD analysis. JEM-2000EX provided transmission electron microscopy. The samples and foils were polished at 50V with an electrolyte consisting of 10 % perchloric acid and 90 % butanol. Axiovert 100A and a microhardness tester MNT-10 with a 100 g load and 10 second time-lag were used for Vickers microhardness tests.

Results and Discussion

The microstructure of SLM Inconel 718

The BSE cross section image of superalloy Inconel 718 in as-built SLM condition is represented in Fig. 1(a). The microstructure consists of coarse and fine γ grains. The size of γ grains is about 20–100 μm. γ grains contain columnar and equiaxed subgrains (Fig. 1(a,b)) [25,26]. The plates of the δ (orthorhombic $D0_a$ structure) phase, small carbides and, probably oxides, are located at the γ grain boundaries. Columnar subgrains consist of submicrocrystalline equiaxed subgrains of about 0.5 μm. Dispersed γ'' (tetragonal $D0_{22}$ structure) and γ' (cubic $L1_2$ structure) particles are precipitated in γ subgrains (Fig. 1(c,d)), like in conventional superalloy [27]. The diffraction pattern of the SLM alloy at Fig. 1(e) shows the existence of Ni-based (γ phase, (331)), orthorhombic Ni_3Nb (δ phase, (313)), body-centered tetragonal Ni_3Nb (γ'' phase, (301)), and Ni_3Al (γ' phase, (222)). EBSD analysis of the initial microstructure, earlier performed in [28], showed that high-angle grain boundaries accounted for 26 %.

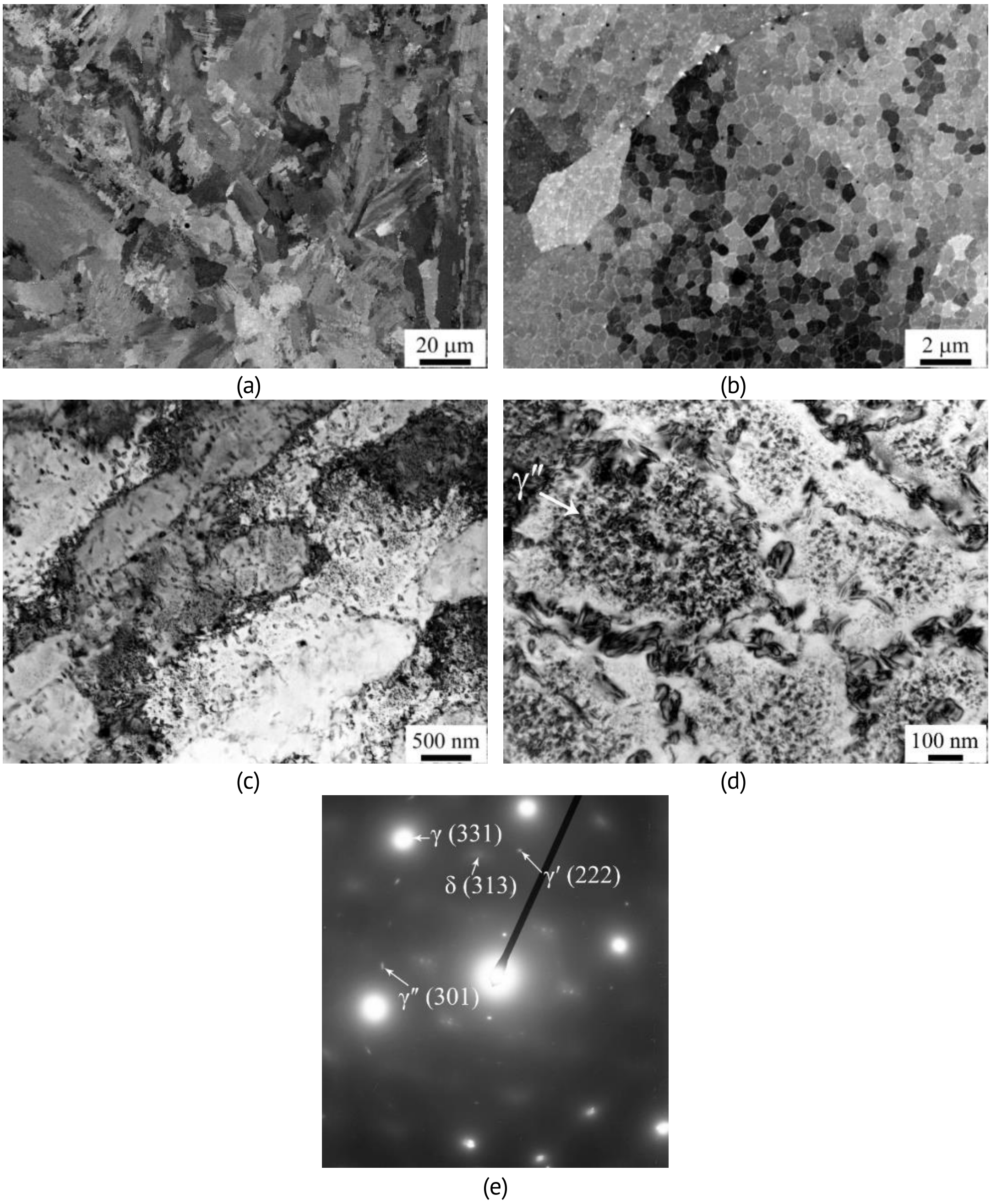

Fig. 1. The microstructure of SLM Inconel 718: BSE images of columnar subgrains and of equiaxed subgrains (a,b); transmission electron microscopy (TEM) images of submicrocrystalline subgrains (c,d); the diffraction pattern of the whole area of Fig. 1(d)

The microstructure of SLM Inconel 718 subjected to HPT

Figure 2 shows BSE and TEM images of SLM Inconel 718 subjected to HPT. The γ grain size in this condition was about 30 nm which is akin to that of conventional alloy subjected to HPT [22,23]. It is well known that the volume fraction of γ' precipitates in conventional Inconel 718 alloy is less than 5 %, γ'' precipitates is less than 25 % [29], and δ phase is about 16 % [30]. Really a large amount of dispersed precipitates as δ phase, carbides and oxides of the SLM alloy is unlikely to dissolve in γ matrix during HPT. Dispersed particles, probably fine carbides or oxides were visible in Fig. 2(a). The diffraction pattern of the alloy after HPT of TEM image Fig. 2(b) showed the existence of orthorhombic Ni_3Nb (δ phase, (211)), as well as Ni-based γ phase, (200). Probably metastable γ'' phase and γ' phase are almost completely dissolved during HPT as in the conventional superalloy subjected to the same treatment [23].

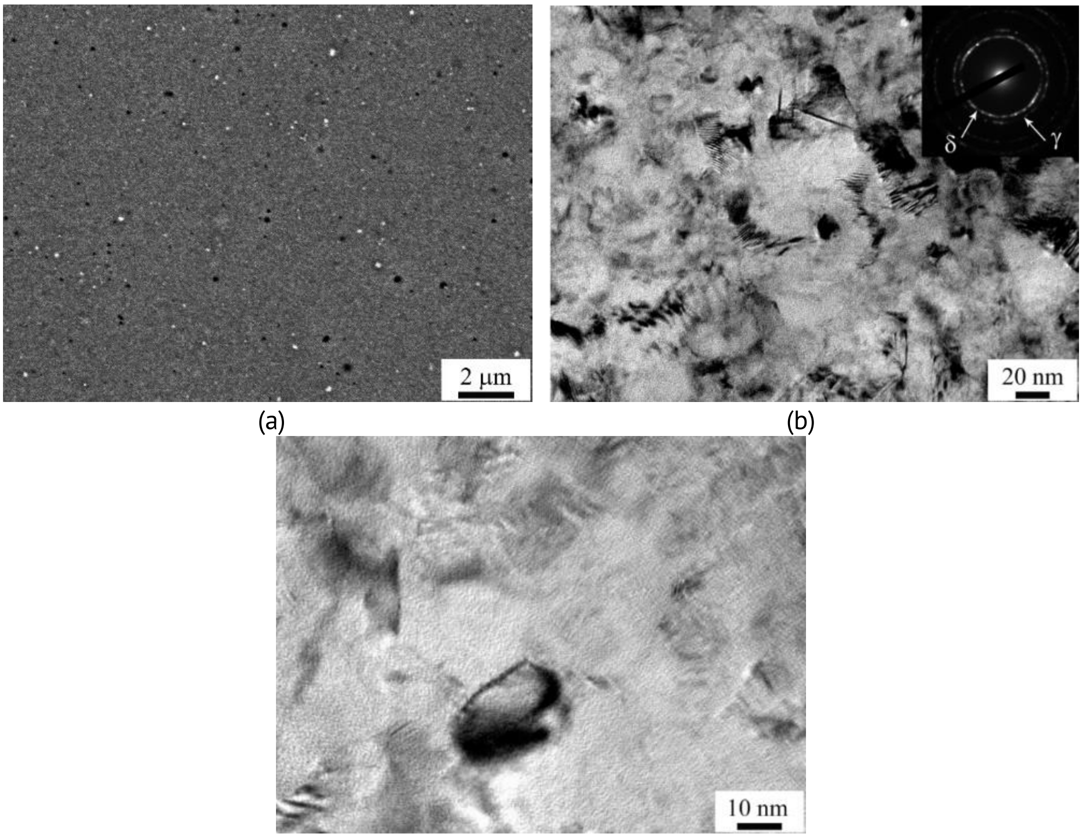

(a) (b) (c)

Fig. 2. Microstructure of SLM Inconel 718 subjected to HPT: BSE image (a), TEM images (b, c) with electron diffraction pattern (b)

The microstructure of SLM Inconel 718 subjected to annealing

Figure 3 shows the BSE images and the EBSD orientation map of SLM Inconel 718 after annealing at 600 °C for 2 h. The quantity of δ phase precipitates, carbides and oxides increased along the grain and subgrain boundaries during annealing (Fig. 3(a,b)). The microstructure contains coarse and fine γ grains. The γ grains also exhibited the presence of both columnar and equiaxed subgrains, while the γ grain size remained unaltered in comparison to the as-built condition (Fig. 1(a,b)). The EBSD orientation map shows that the quantity of low angle boundaries decreased (Fig. 3(c)) and the fraction of high angle boundaries increased during annealing up to 69 % (Fig. 3(d)). The Σ3 twin boundaries were not identified in either the BSE images or the misorientation – angle distribution for grain boundaries (about 60°) after annealing (Fig. 3).

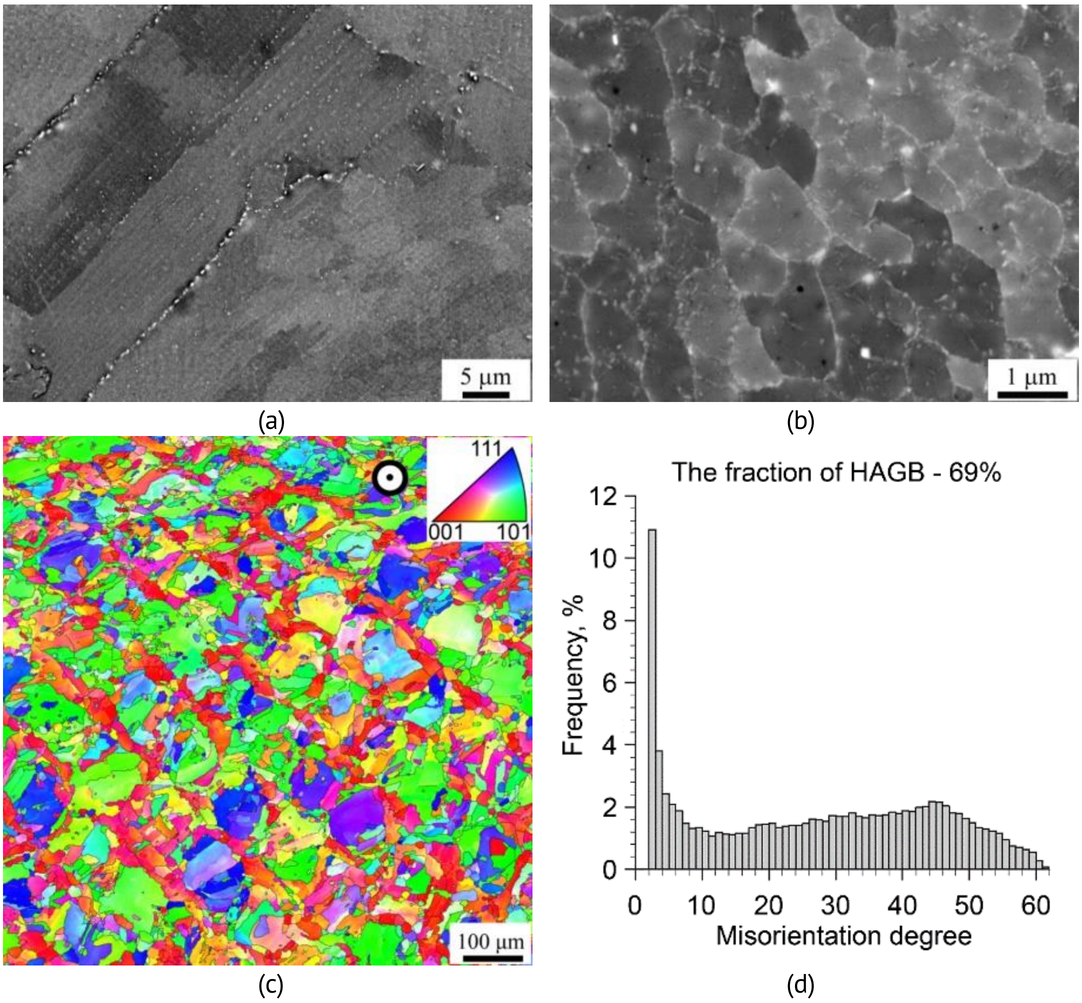

Fig. 3. The microstructure of SLM Inconel 718 after annealing at 600 °C for 2 hours: BSE images (a,b), EBSD normal-direction (inverse-pole-figure) orientation map (c) and corresponding misorientation – angle distribution for grain boundaries (d), and the circle in (c) indicates the plane is perpendicular to the build direction

The microstructure of SLM Inconel 718 subjected to HPT and annealing

Figure 4 represents the TEM images of the sample subjected to HPT and annealing at 600 °C for 2 hours. The average size of γ grains increased from 30 to 50 nm. The diffraction pattern of the SLM alloy subjected to HPT and annealing exhibited the presence of the orthorhombic δ phase (412) and the γ phase (220), as observed in Fig. 4(b). γ phase and δ phase precipitates were revealed in the microstructure. The γ'' precipitates were dissolved in the γ matrix during HPT and subsequently precipitated during annealing by additional δ-phase particles. HPT and annealing of the SLM alloy resulted in the microstructure similar to that of the conventional superalloy subjected to the same treatment [22,23].

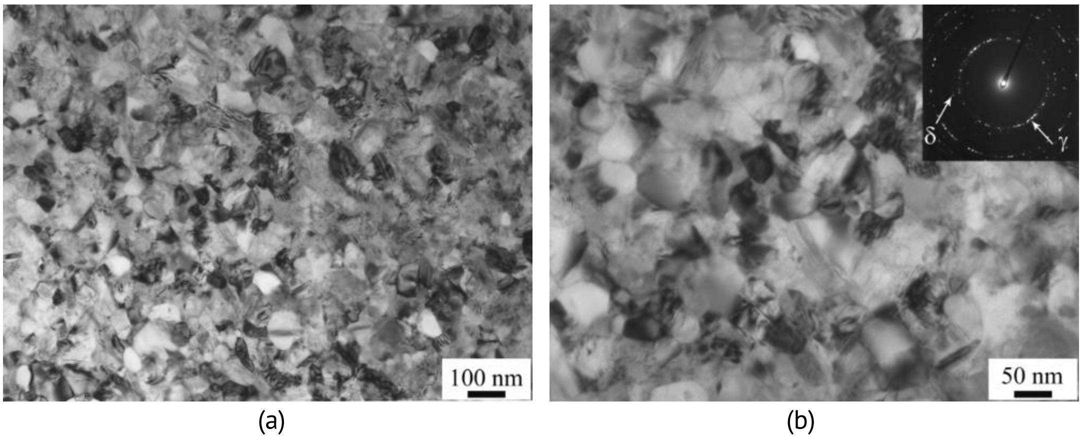

Fig. 4. The microstructure of SLM Inconel 718 subjected to HPT and annealing at 600 °C for 2 hours: TEM images (a,b) with electron diffraction pattern (b)

Effect of HPT and annealing on the microhardness

The microhardness (HV) of SLM and conventional Inconel 718 in different conditions is represented in Table 2. The SLM superalloy that was the subject of this investigation exhibited a microhardness of 530.23 ± 19.37 HV, which is higher than the microhardness of 432 ± 12 HV reported in [31]. Annealing at 600 °C for two hours did not impact the microhardness of the SLM alloy, due to the previous treatment of the alloy being carried out at a higher temperature via laser melting, followed by cooling. As shown in [32], the γ'' phase in SLM alloy is precipitated at temperatures of 700 °C and above. It can be reasonably assumed that the annealing temperature of 600 °C was too low to precipitate the γ'' phase in the SLM alloy. Indeed, the minimum aging temperature for Inconel 718 alloy is typically 620 °C [33]. The conventional superalloy microhardness is observed to decrease to 477.21 HV as a consequence of a reduction in dislocation density following hot forging and subsequent annealing. Better microhardness after HPT is related with microstructure refinement down to the nanocrystalline level. The observed increase in microhardness following subsequent annealing is likely attributable to the precipitation of the δ phase and the onset of polygonization that occurred prior to recrystallization [34]. The microhardness of SLM Inconel 718 is higher than that of the conventional alloy, probably due to dispersed oxides and carbides in the SLM alloy at the grain boundaries [35].

Table 2. Microhardness (HV) of SLM Inconel 718 and conventional Inconel 718 subjected to different treatment

Conditions	**Inconel 718**	**SLM Inconel 718**
Initial	547.57 ± 25.49	530.23 ± 19.37
Annealing at 600 °C	477.21 ± 19.37	528.19 ± 12.24
HPT	637.30 ± 39.77	721.93 ± 26.51
HPT+annealing at 600 °C	866.73 ± 42.83	956.46 ± 25.49

Conclusions

1. The stable δ phase precipitates present in the SLM Inconel 718 alloy did not fully dissolve during HPT, and their presence was more clearly discernible following annealing at 600 °C for 2 h.

2. The mean size of γ grains increased from 30 to 50 nm during annealing at 600 °C for 2 h of the SLM Inconel 718 alloy subjected to HPT on five revolutions.
3. The SLM Inconel 718 processed by HPT on five revolutions and annealed at 600 °C for 2 h show the higher microhardness (956.46 HV) than conventional one (866.73 HV), and in both cases was achieved in due to additional precipitation by dispersed δ phase.

CRediT authorship contribution statement

Kamilla Sh. Mukhtarova: investigation, writing – original draft, data curation; **Ruslan V. Shakhov**: investigation; **Shamil Kh. Mukhtarov**: conceptualization, writing – review & editing.

Conflict of interest

The authors declare that they have no conflict of interest.

References

1. Schafrik R, Sprague R. Superalloy technology – a perspective on critical innovations for turbine engines. *Key Engineering Materials*. 2008;380: 113–134.
2. Special Metals Corporation. *INCONEL alloy 718*. Available from: *https://www.specialmetals.com/documents/technical-bulletins/inconel/inconel-alloy-718.pdf* [Accessed 20th November 2024].
3. Maslov AA, Nazarov AY, Khusainova AM, Ramazanov KN. Y–Al–O Coating Grown on Inconel 718 Alloy. *Physics of Metals and Metallography*. 2024;125: 1609–1614.
4. DebRoy T, Wei HL, Zuback JS, Mukherjee T, Elmer JW, Milewski JO, Beese AM, Wilson-Heid A, De A, Zhang W. Additive manufacturing of metallic components – Process, structure and properties. *Progress in Materials Science*. 2018;92: 112–224.
5. Yap CY, Chua CK, Dong ZL, Liu ZH, Zhang DQ, Loh LE, Sing SL. Review of selective laser melting: Materials and applications. *Applied Physics Reviews*. 2015;2(4): 041101.
6. Oliveira JP, Santos TG, Miranda RM. Revisiting fundamental welding concepts to improve additive manufacturing: from theory to practice. *Progress in Materials Science*. 2020;107: 100590.
7. Körner C. Additive manufacturing of metallic components by selective electron beam melting – a review. *International Materials Reviews*. 2016;61(5): 361–377.
8. Tucho WM, Cuvillier P, Sjolyst-Kverneland A, Hansen V. Microstructure and hardness studies of Inconel 718 manufactured by selective laser melting before and after solution heat treatment. *Materials Science and Engineering: A*. 2017;689: 220–232.
9. Kuo YL, Kakehi K. Influence of powder surface contamination in the Ni-based superalloy Alloy718 fabricated by selective laser melting and hot isostatic pressing. *Metals*. 2017;7(9): 367.
10. Lu Y, Wu S, Gan Y, Huang T, Yang C, Junjie L, Lin J. Study on the microstructure, mechanical property and residual stress of SLM Inconel-718 alloy manufactured by differing island scanning strategy. *Optics & Laser Technology*. 2015;75: 197–206.
11. Polozov IA, Borisov EV, Sufiiarov VSh, Popovich AA. Selective laser melting of copper alloy. *Materials Physics and Mechanics*. 2020;43(1): 65–71.
12. Murr LE, Martinez E, Amato KN, Gaytan SM, Hernandez J, Ramirez DA, Shindo PW, Medina F, Wicker RB. Fabrication of metal and alloy components by additive manufacturing: examples of 3D materials science. *Journal of Materials Research and Technology*. 2012;1(1): 42–54.
13. Popovich AA, Sufiiarov VSh, Borisov EV, Polozov IA, Masaylo DV. Design and manufacturing of tailored microstructure with selective laser melting. *Materials Physics and Mechanics*. 2018;38(1): 1–10.
14. Raza T, Andersson J, Svensson LE. Microstructure of selective laser melted Alloy 718 in as-manufactured and post heat treated condition. *Procedia Manufacturing*. 2018;25: 450–458.
15. Gong X, Wang X, Cole V, Jones Z, Cooper K, Chou K. Characterization of Microstructure and Mechanical Property of Inconel 718 From Selective Laser Melting. In: *ASME 2015 International Manufacturing Science*

and Engineering Conference: Volume 1: Processing, 8–12 June 2015, Charlotte, North Carolina, USA. American Society of Mechanical Engineers; 2015. MSEC2015-9317, V001T02A061.
16. Popovich AA, Sufiiarov VSh, Polozov IA, Borisov EV. Microstructure and mechanical properties of Inconel 718 produced by SLM and subsequent heat treatment. *Key Engineering Materials.* 2015;651–653: 665–670.
17. Raghavan S, Zhang B, Wang P, Sun CN, Nai MLS, Li T, Wei J. Effect of different heat treatments on the microstructure and mechanical properties in selective laser melted INCONEL 718 alloy. *Materials and Manufacturing Processes.* 2017;32(14): 1588–1595.
18. Mukhtarova KS, Shakhov RV, Mukhtarov SK, Smirnov VV, Imayev VM. Microstructure and mechanical properties of the Inconel 718 superalloy manufactured by selective laser melting. *Letters on Materials.* 2019;9(4): 480–484.
19. Wei W, Xiao JC, Wang CF, Cheng Q, Guo FJ, He Q, Wang MS, Jiang SZ, Huang CX. Hierarchical microstructure and enhanced mechanical properties of SLM-fabricated GH5188 Co-superalloy. *Materials Science & Engineering A.* 2022;831: 142276.
20. Zeng Q, Wang K, Lu S, Lu C, Wang Z, Zhou T. Evolution of the microstructure and multi-objective optimization of the tensile properties of GH3625 superalloy by selective laser melting. *Journal of Materials Research and Technology.* 2023;24: 8826–8848.
21. Liu H, Han S, Lan Y, Zhao W, Zhang C, Li Q. The effect of direct aging treatment on microstructure and mechanical properties of the GH4099 superalloys produced by selective laser melting. *Journal of Alloys and Compounds.* 2024;1007: 176493.
22. Sauvage X, Mukhtarov S. Microstructure evolution of a multiphase superalloy processed by severe plastic deformation. *IOP Conference Series: Materials Science and Engineering.* 2014;63: 012173.
23. Mukhtarov ShKh, Sauvage X. Microstructure and microhardness of a nanostructured nickel-iron based alloy. *Materials Science Forum.* 2011;683: 127–135.
24. Gunderov DV, Asfandiyarov RN, Raab GI, Churakova AA, Astanin VV. Method for slippage evaluation at various stages of high-pressure torsion and its application to Fe-0.1%C. *Letters on Materials.* 2021;11(4): 416–421.
25. Zhou S, Liu L, Yang Y, Lv P. Effect of heat treatment on the microstructure and recrystallization of an SLM nickel-based superalloy. *Materials Today Communications.* 2024;39: 109253.
26. Wang H, Wu D, Xiao F, Quan G, Liu B. Influence of heat treatment temperature on grain structures and properties of a Ni-based superalloy fabricated via selective laser melting. *Materials Today Communications.* 2024;41: 110673.
27. Burke MG, Miller MK. Precipitation in Alloy 718: A combined AEM and APFIM investigation. In: Loria EA. (eds.) *Superalloys 718, 625 and Various Derivatives.* Warrendale PA: The Minerals, Metals & Materials Society; 1991. p. 331–350.
28. Shakhov R, Mukhtarova K. Nb rich precipitates in Inconel 718 produced by selective laser melting. *Letters on Materials.* 2018;8(1): 105–109.
29. Yang L, Chang KM, Mannan S, deBarbadillo J. A new DTA approach for verifying precipitate solvus in Inconel alloy 718. In: Loria EA. (eds.) *Superalloys 718, 625, 706 and Various Derivatives.* Warrendale PA: The Minerals, Metals & Materials Society; 1997. p. 353–365.
30. Moyye DP, Satheesh Kumar SS, Nagarajan D, Balasundar I. Microstructural evolution and mechanical behavior during isothermal multiaxial forging of nickel-based Superalloy SUPERNI 718. To be published in *Journal of Materials Engineering and Performance.* [Preprint] 2024. Available from: doi.org/10.1007/s11665-024-09249-1
31. Protatskaya AA, Sharipova SR. The effect of heat treatment on the structure of the SLM of the Inconel 718 alloy. *Materials. Technologies. Design.* 2022;4(2): 46–51.
32. Ghaemifar S, Mirzadeh H. Precipitation kinetics of gamma double prime phase during direct aging treatment of Inconel 718 superalloy additively manufactured by selective laser melting. *Journal of Materials Research and Technology.* 2023;27: 4248–4255.
33. Chen B, Zhuo L, Xie Y, Huang S, Wang T, Yan T, Gong X, Wang Y. Comparative study on microstructure, mechanical and high temperature oxidation resistant behaviors of SLM IN718 superalloy before and after heat treatment. *Journal of Materials Research and Technology.* 2024;31: 1535–1546.
34. Mukhtarov ShKh. Effect of grain size on the superplastic behavior of a nanostructured nickel-based superalloy. *Materials Science Forum.* 2009;633–634: 569–575.
35. Sheinerman AG. Strengthening of nanocrystalline alloys by grain boundary segregations. *Materials Physics and Mechanics.* 2022;50(2): 193–199.